Electrochimica Acta 541 (2025) 147346

Contents lists available at ScienceDirect

Electrochimica Acta

journal homepage: www.journals.elsevier.com/electrochimica-acta

Enhancing the inhibition of localised corrosion on a pre-rusted steel surface by the synergistic effect of rare-earth and inorganic inhibitors

Medhani Pathirana [a], Majid Laleh [a,b], Anthony Somers [c], Bruce Hinton [c], Glen B. Deacon [d], Peter C. Junk [e], Mike Yongjun Tan [a,c,*]

[a] School of Engineering, Deakin University, Waurn Ponds, VIC 3216, Australia
[b] ARC Research Hub for Australian Steel Innovation, University of Wollongong, Wollongong, NSW 2522, Australia
[c] Institute for Frontier Materials, Deakin University, Waurn Ponds, VIC 3216, Australia
[d] School of Chemistry, Monash University, Clayton Campus, VIC 3800, Australia
[e] College of Science & Engineering, James Cook University, Townsville, Qld 4811, Australia

ARTICLE INFO

Keywords:
Waterline corrosion
Localised corrosion
Electrochemical measurements
EIS
Polarisation
Corrosion inhibition
Rare-earth metal inhibitors

ABSTRACT

Waterline corrosion of steel, particularly on pre-rusted surfaces, presents a significant challenge in marine and industrial environments due to its localised and aggressive nature. This study investigates the effectiveness of rare-earth metal (REM) carboxylate inhibitors, i.e., lanthanum 4-hydroxycinnamate ($La(4OHcin)_3{\cdot}5H_2O$), yttrium 3-(4′-methylbenzoyl)propanoate ($[Y(mbp)_3(H_2O)]$), and yttrium 4-hydroxybenzoate ($[Y_2(4hob)_6(H_2O)_4].2H_2O$), in mitigating localised corrosion on pre-rusted steel partially immersed in simulated seawater. *In-situ* galvanic current mapping coupled with local electrochemical impedance spectroscopy (EIS) and potentiodynamic polarisation measurements were facilitated using a wire beam electrode (WBE). While these REM inhibitors demonstrated high inhibition efficiency (>90 %) on fresh steel, their efficiency on pre-rusted steel was significantly lower (~40–49 %), indicating a critical influence ofrust layers on inhibitor performance. Efforts to improve inhibitor penetration through the rust layers using smaller-molecule inhibitors showed minimal benefit. However, when REM inhibitors were combined with sodium molybdate, an inorganic anodic inhibitor with buffering capacity, the inhibition efficiency increased substantially, reaching up to 69 %. Local EIS measurements confirmed enhanced inhibitor film resistance and more uniform inhibitor distribution with the mixed inhibitors. These results suggest a synergistic mechanism where REM carboxylates provide cathodic and anodic protection through adsorption and hydroxide precipitation, while sodium molybdate stabilises the environment and reinforces the passive film. This study highlights the limitations of single-component inhibitors for pre-rusted steel surfaces and demonstrates the potential of hybrid organic–inorganic inhibitor systems for effective corrosion mitigation at the waterline.

1. Introduction

Corrosion inhibitors are widely used for general corrosion control in industry, however the application of inhibitors for localised corrosion control is very limited. This is because a locally corroding metal surface has separated anodic and cathodic areas where the local surface chemistry can change with the processes of corrosion. For instance, the cathodic area can develop a higher local pH value due to oxygen reduction reactions, while the anodic area could have a lower local pH value due to hydrolysis of metallic ions, and a rust layer could form between anodic and cathodic areas. The formation of the rust layer can further change the corrosion environment; it was shown that crevice corrosion could occur under the rust layer [1–4]. These factors make the inhibition of localised corrosion, especially on pre-rusted surfaces, very difficult. However, in industry practice most engineering structures have some pre-rust layers presence and are exposed to nonuniform environmental conditions. For instance, rusting is commonly observed at the waterline areas of hulls of retired ships [5], on internal surfaces of nuclear waste tanks [6,7], on internal and external pipelines [8], and on steel piling [9]. Localised forms of corrosion can induce premature failure of industrial structures because localised corrosion damage commonly occurs at stress concentrated areas where fracture may then

* Corresponding author at: School of Engineering, Deakin University, Waurn Ponds, VIC 3216, Australia.
E-mail address: mike.tan@deakin.edu.au (M.Y. Tan).

https://doi.org/10.1016/j.electacta.2025.147346
Received 6 July 2025; Received in revised form 25 August 2025; Accepted 7 September 2025
Available online 8 September 2025

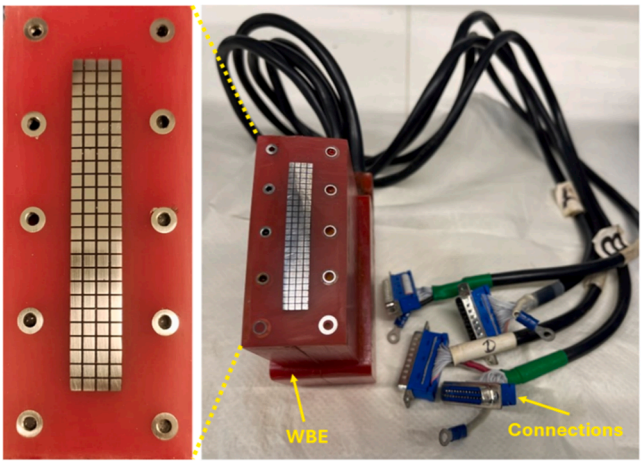

Fig. 1. Photographs of the WBE and its connections indicating the arrangement of 100 individual square electrodes.

occur [10,11].

Waterline corrosion is selected in this work as a typical form of localised corrosion because it is a complex, significant and difficult to control form of localised corrosion [6–9]. Since Evans in the 1940s investigated this type of corrosion on steel and zinc which were submerged partially in NaCl solution [12], significant effort has been made to understand and control waterline corrosion in various environmental conditions. Waterline corrosion is generally considered to be due to electrochemical processes and activities occurring in an oxygen differential aeration cell. The areas above and around the waterline become corrosion cathodes while the area below the waterline become anodes [13–17]. The actual mechanism and influencing factors can be much more complex. Many environmental factors have also been found to affect waterline corrosion [18–26]. Different waterline corrosion behaviours were reported to occur on carbon steel partially immersed in a 3.5 wt % NaCl solution (simulating seawater) [20,24], in Evans solution [25], in artificial and natural seawater [21], and in the ocean [18,19]. Furthermore, the presence of microbes in natural seawater [21], the flowing of electrolyte [24], the depth of water [22], and the inhibition ability of a particular solution [26] were also found to be factors affecting waterline corrosion. Another important factor that was found to play a vital role in the waterline corrosion process and mechanisms is the rust layer [1]. It was shown in the previous study [1] that the rust layer plays a major role in waterline corrosion by forming a crevice where crevice corrosion occurs. It was also reported that although the initiation and propagation of waterline corrosion is controlled by concentration and diffusion of dissolved oxygen, the deceleration stage is controlled by the presence of rust [20]. Even though these studies [1,20] have shown the effect of rust on the waterline corrosion process, no studies have been carried out (i) on the effect of the rust layer on the inhibition of waterline corrosion, and (ii) on the ability of inhibitors to control waterline corrosion on a pre-rusted steel surface.

Over the past decades, a major research focus has been on the discovery and development of non-toxic, environmentally friendly and effective inhibitors to control general corrosion in various situations. Hinton et al. discovered that Rare Earth Metal (REM) salts such as $CeCl_3$ reduced corrosion on mild steel exposed to tap water by forming a precipitate at cathodic sites and thereby affecting the cathodic reaction and the corrosion process [27,28]. Mercer et al. had shown that carboxylic acids can form a protective film over anodic sites on steel by adsorption leading to a reduction in the anodic reaction and inhibition of corrosion [29]. Many researchers then developed REM-based corrosion inhibitors including bifunctional corrosion inhibitors by combining REM salts with organic ligands such as carboxylates and phosphate esters [30–41]. Recently the efficiency of REM inhibitors, La(4OHcin)$_3$·5H$_2$O and [Y(mbp)$_3$(H$_2$O)], for localised corrosion inhibition was investigated [42]. It has been shown that La(4OHcin)$_3$·5H$_2$O efficiently mitigated general corrosion on fully submerged steel [30–36], and that La(4OHcin)$_3$·5H$_2$O was an effective inhibitor for the early stages of localised corrosion at the waterline on a fresh steel surface with no rust present [42]. However, La(4OHcin)$_3$·5H$_2$O was a poor inhibitor as it exacerbated localised corrosion with time, whereas [Y(mbp)$_3$(H$_2$O)] was more effective with time [42]. However, it should be noted that two major issues remained unaddressed: (i) no inhibitor has been tested for their effectiveness with pre-corroded steel, and (ii) the

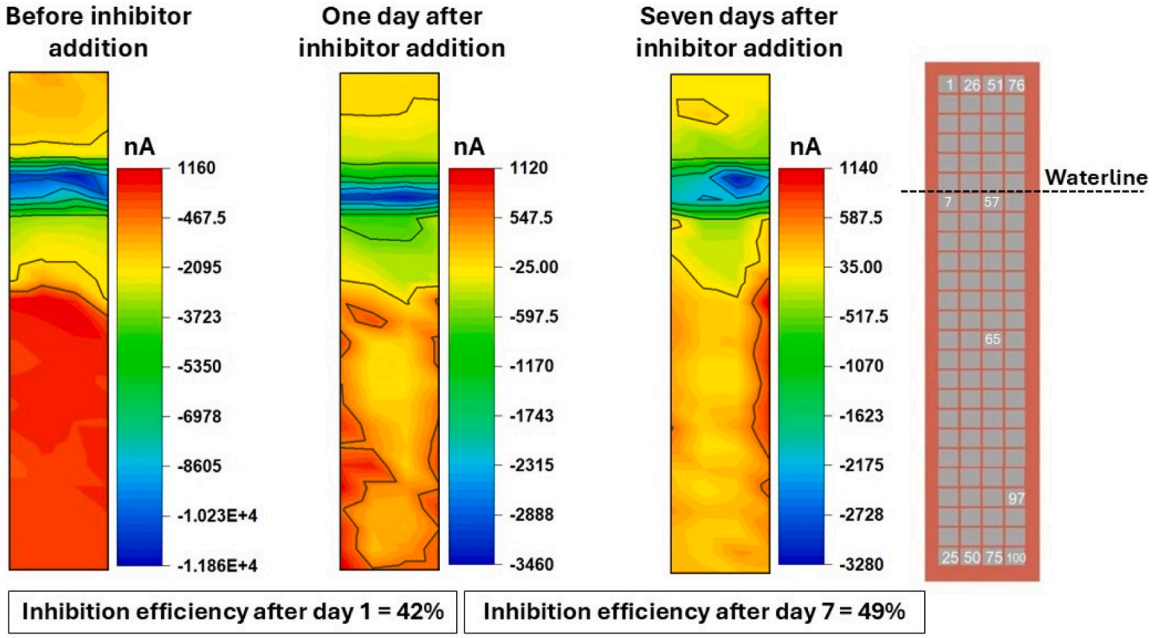

Fig. 2. Galvanic current distribution maps before, one day after, and seven days after adding La(4OHcin)$_3$·5H$_2$O inhibitor to the 3.5 wt % NaCl solution. Note that before adding the inhibitor, the WBE probe was corroded for 14 days under the waterline corrosion conditions. Schematic illustration of the WBE probe is also presented to indicate the location of electrodes where the local potentiodynamic polarisations measurements are done.

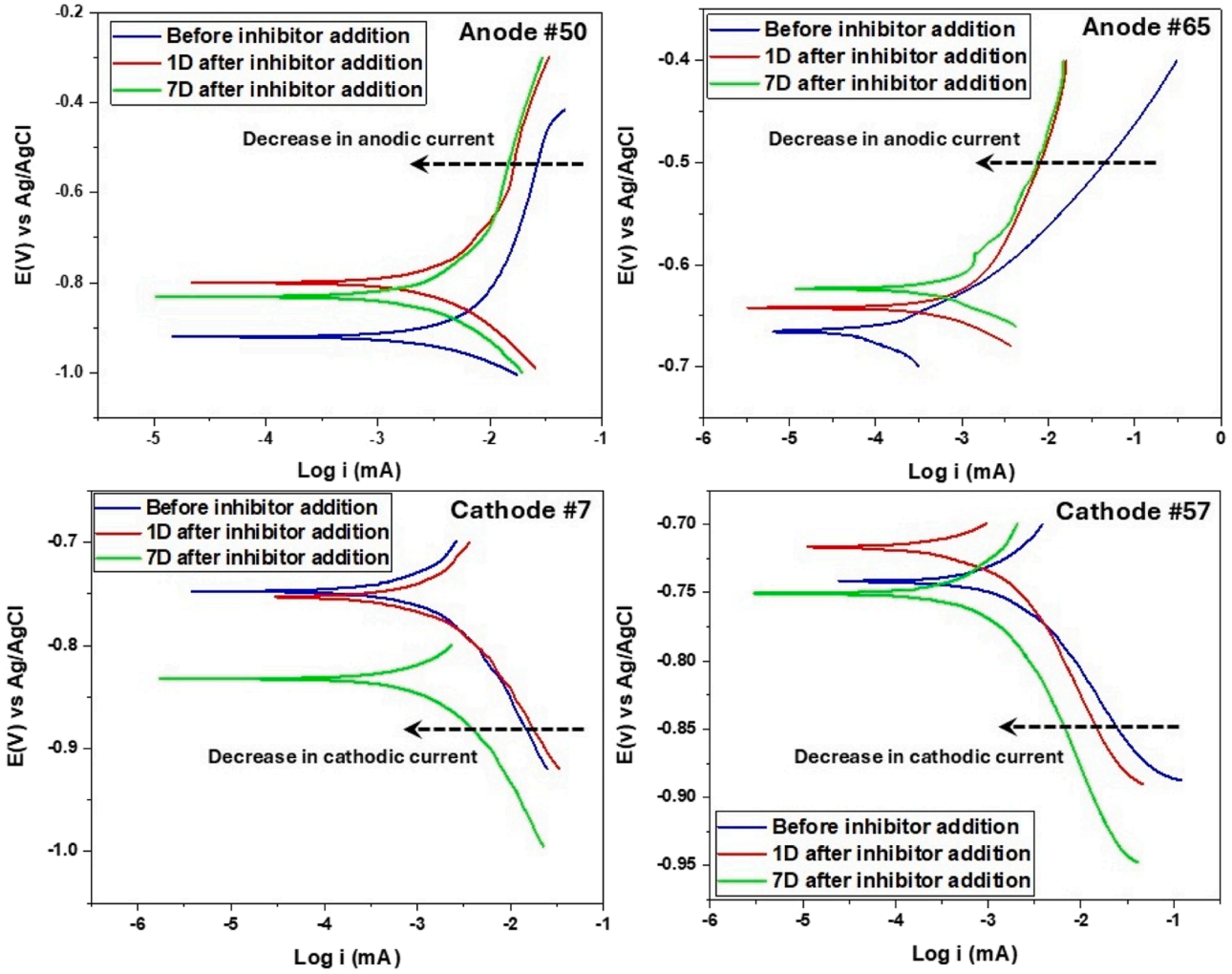

Fig. 3. Local potentiodynamic polarisation curves measured on the representative local anodic sites #50 and #65 and local cathodic sites #7 and #57 before, one day after, and seven days after addition of La(4OHcin)$_3$·5H$_2$O inhibitor to 3.5 wt % NaCl solution. To see the location of the anodic and cathodic electrodes, please refer to the schematic of the WBE in Fig. 2.

effect of a rust layer on the inhibition process has not been studied.

This present work explores the application of environmentally friendly REM inhibitors for inhibiting waterline corrosion on pre-rusted steel surfaces, and new approaches to enhancing localised corrosion inhibition of pre-rusted steel. REM inhibitors with different molecular features and sizes including [Y$_2$(4hob)$_6$(H$_2$O)$_4$].2H$_2$O, La(4OHcin)$_3$·5H$_2$O, and [Y(mbp)$_3$(H$_2$O)] [36,39,43] were selected for study, and the possible synergistic effect of inhibitors has been further explored by mixing REM and inorganic inhibitor sodium molybdate. This work focuses on the need to develop corrosion inhibitors that can mitigate localised corrosion on pre-rusted metal surfaces to prevent premature failure of industrial infrastructure.

2. Materials and methods

A major difficulty in studying localised corrosion and its inhibition is the limitations with conventional techniques in performing *in-situ* measurement and monitoring of the initiation, propagation and inhibition of localised corrosion. To quantify the behaviour, efficiency and effects of inhibitors on localised corrosion processes, it is especially important to have a technique which can measure *in-situ* and monitor local electrochemical changes, and the effects inhibitors on the local galvanic current flows between local anodic and cathodic sites, variations in local electrode potential and changes in local impedance. These changes in local areas cannot be observed and measured using conventional techniques such as weight loss measurements, conventional polarisation measurements and EIS, which give information from the overall electrode surface. Indeed, they are unable to measure local events. To address these difficulties, an electrochemically integrated multi-electrode array probe, often referred to as the wire beam electrode (WBE), was used to obtain *in-situ* electrochemical measurements. More specific details of this technique and the experimental setup have been reported in previous studies [1,42,44].

In this study, a WBE was used which consisted of 100 square electrodes mounted in epoxy resin. All 100 electrodes were arranged in an array of 25 rows with 4 per row as shown in Fig. 1. The dimensions of a single electrode was 2.3 mm × 2.3 mm. The material of the electrodes was X65 carbon steel, and the composition was 0.04 C, 0.2 Si, 1.5 Mn, 0.011 P, 0.003 S, 0.02 Mo, and Fe balance (wt %). The 100 electrodes simulated a continuous steel surface by connecting electrically. The WBE was partially immersed in the test solution such that 19 rows were exposed to the test solution (below the waterline) and 6 rows were exposed to air (above the waterline) to simulate the waterline corrosion condition. This setup can detect corrosion at local areas, and it continuously monitors corrosion for long exposure times over the electrode array surface. This is an improved technique for studying localised corrosion and its inhibition at waterline because it overcomes the limitations of probing localised corrosion by conventional methods.

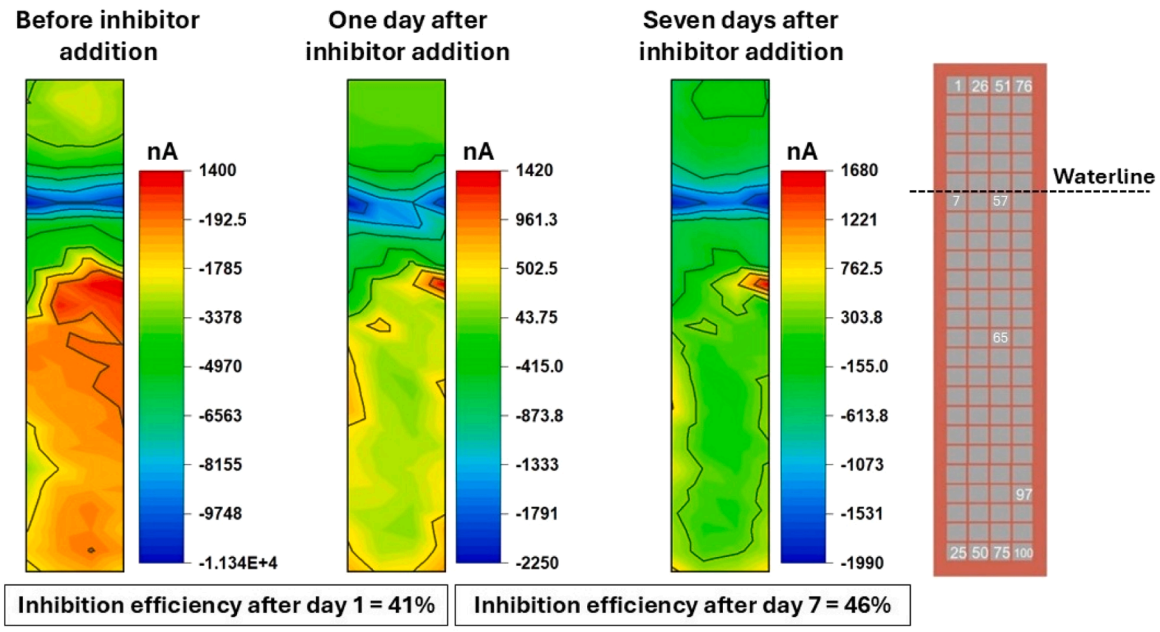

Fig. 4. Galvanic current distribution maps before, one day after, and seven days after adding [Y(mbp)$_3$(H$_2$O)] inhibitor to the 3.5 wt % NaCl solution. Note that before adding the inhibitor, the WBE probe was corroded for 14 days under the waterline corrosion conditions. Schematic illustration of the WBE probe is also presented to indicate the location of electrodes where the local potentiodynamic polarisations measurements are done.

It has been reported that REM inhibitors such as La(4OHcin)$_3$·5H$_2$O and [Y(mbp)$_3$(H$_2$O)] can efficiently mitigate general corrosion on fully submerged steel [30–36]. In the previous work [42], it was demonstrated that La(4OHcin)$_3$·5H$_2$O achieved over 90 % inhibition efficiency on fresh steel surfaces at the waterline. In this study, that investigation is extended to a pre-rusted steel to determine whether the inhibitor can similarly mitigate established localised corrosion. To this end, La(4OHcin)$_3$·5H$_2$O was introduced into a 3.5 wt % NaCl solution after the WBE probe had been allowed to corrode for 14 days in a similar manner as described in references [1,42].

Before every experiment, the electrode array surface was ground to a 1200 grit finish using a range of silicon carbide abrasive papers. Then, the probe was cleaned with ethanol and dried using hot air. The electrode array was exposed to a 3.5 % wt % NaCl solution (pH ~ 7) for 14 days to establish the localised corrosion, and for rust layers to form on the electrode array surface. After 14 days of exposure, inhibitors [39,43,45] were added to the test solution. The following inhibitors were used in this study, 1 mmol/l of La(4OHcin)$_3$·5H$_2$O, 1 mmol/l of [Y(mbp)$_3$(H$_2$O)], 1 mmol/l of [Y$_2$(4hob)$_6$(H$_2$O)$_4$].2H$_2$O, 100 mmol/l of sodium molybdate, inhibitor mixture (1 mmol/l of La(4OHcin)$_3$·5H$_2$O + 100 mmol/l of sodium molybdate) and inhibitor mixture (1 mmol/l of [Y(mbp)$_3$(H$_2$O)] + 100 mmol/l of sodium molybdate). All solutions were prepared using analytical-grade reagents (Sigma Aldrich) and deionised water. All rare earth metal (REM) complexes were synthesised according to established literature procedures [39,43,45]. Sodium molybdate was selected because it could enhance anodic inhibition by acting as a buffering agent in an acidic environment and by forming a passive film over anodic sites [46,47]. After adding an inhibitor, measurements were obtained continuously for another 7 days. Test solutions were prepared freshly for each experiment and the volume of the test solution was 3 litres. The position of the waterline changed due to evaporation of water during the long exposure time. To overcome this issue and maintain the waterline at the same position, distilled water was added periodically. All experiments were conducted for 21 days (first 14 days without inhibitor and another 7 days with inhibitor) at room temperature and under static conditions.

Galvanic currents between anodes and cathodes were obtained continuously during each experiment, and maps showing the distribution of those currents across the array were produced. Each current measurement cycle took approximately 5 min. Local anodic and cathodic sites could be identified based on the galvanic current. Positive current represents anodic sites, and negative current represents cathodic sites. Total anodic currents were calculated by summing all the positive currents. Inhibitor efficiency was calculated using total anodic current as described in Eq. (1).

$$\text{Inhibition efficiency} = \frac{\text{Total anodic current (before adding inhibitor)} - \text{Total anodic current (after adding inhibitor)}}{\text{Total anodic current (before adding inhibitor)}} \times 100\% \quad (1)$$

It should be noted that for each measurement cycle, the total anodic current and total cathodic current across the WBE were compared to verify current conservation. In all experiments, the absolute difference between anodic and cathodic totals was typically <15 % of the total current, corresponding to less than ~2000 nA. These deviations are within the expected limits of the current instrument used in this work. The current instrument measures the currents from each electrode in sequence, i.e. currents are not measured exactly the same time, and therefore some changes in current values could occur during the measurement period of 5 min due to the changing nature of corrosion process. There are also instrument resolution limits, background noise, and current transients when switching electrodes during measurements. Further development of the measurement instrument is in progress to avoid these limitations by measuring all currents simultaneously.

The WBE design ensures that currents are comprehensively

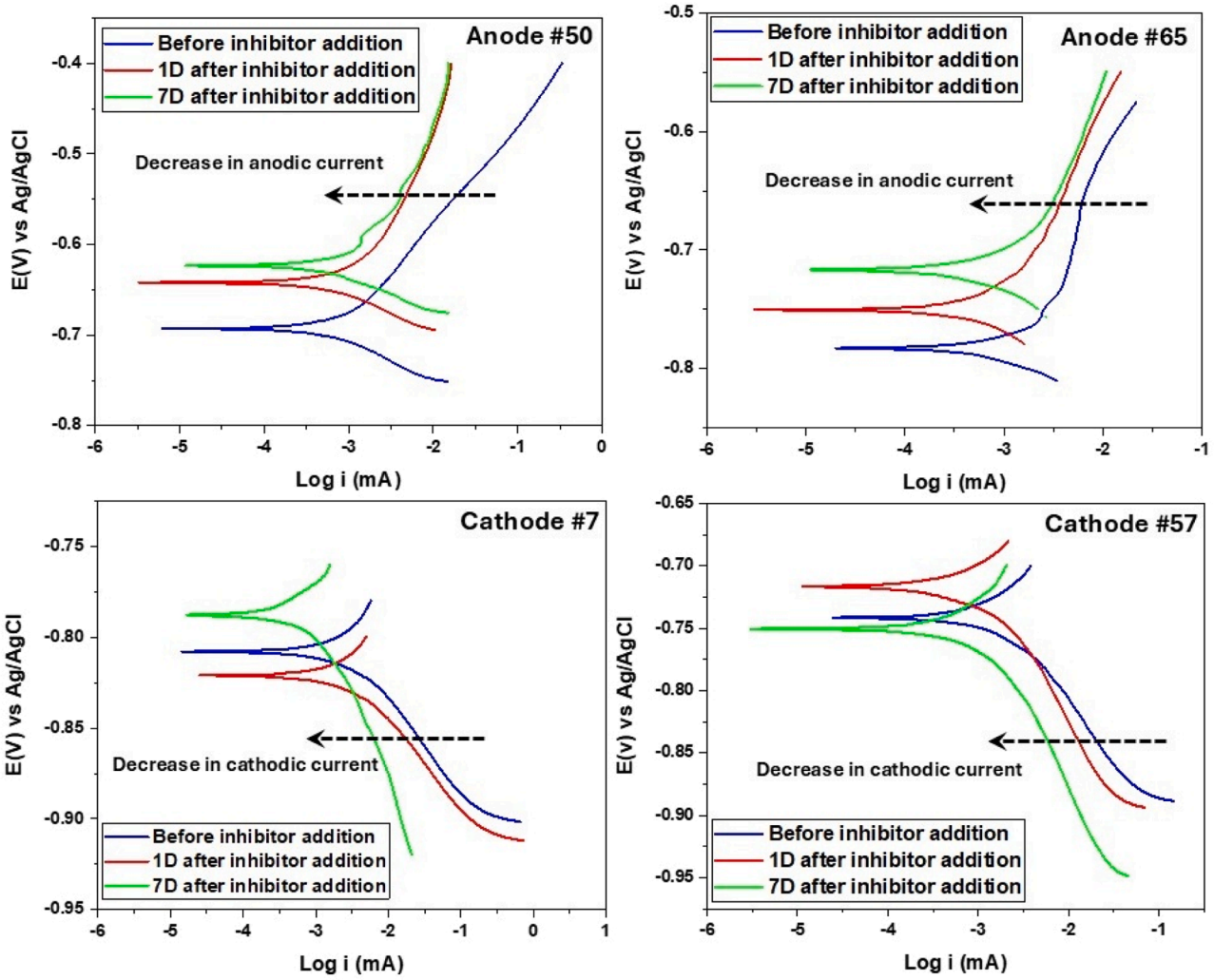

Fig. 5. Local potentiodynamic polarisation curves measured on the representative local anodic sites #50 and #65 and local cathodic sites #7 and #57 before, one day after, and seven days after addition of $[Y(mbp)_3(H_2O)]$ inhibitor to 3.5 wt % NaCl solution. To see the location of the anodic and cathodic electrodes, please refer to the schematic of the WBE in Fig. 4.

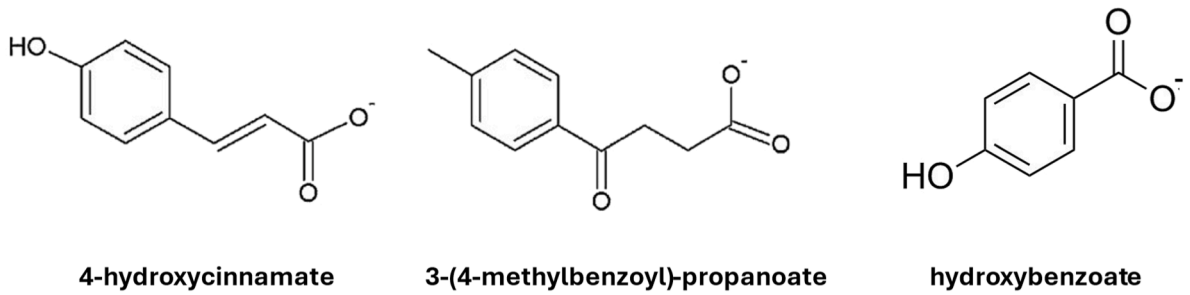

Fig. 6. Chemical structure of inhibitor anions used in this study.

inventoried. In our experiments, since the waterline corrosion system is extremely highly localised, the effects of 'internal' currents flowing within each wire on galvanic current measurement accuracy is minimal because in highly localised corrosion systems, the 'crossing' electrode currents are dominating [14,25]. Summation of total anodic and cathodic currents across the array consistently confirmed near balance, with differences typically <15 %, thereby verifying that essentially all faradaic processes on the electrode surface were captured. This approach has also been validated in prior WBE studies of highly localised corrosion on steel in chloride solutions [14,24,25].

Local potentiodynamic polarisation measurements and local electrochemical impedance spectroscopy (EIS) measurements were carried out to study inhibition mechanisms. Local potentiodynamic polarisation measurements provide information about the local electrochemical changes at anodes and cathodes. At local electrodes, polarisation measurements were carried out before adding each inhibitor, and then after one day and seven days with the inhibitor present. To obtain local polarisation measurements, each electrode of interest was disconnected electrically from the array and connected to the potentiostat as the working electrode. An Ag/AgCl electrode was the reference electrode,

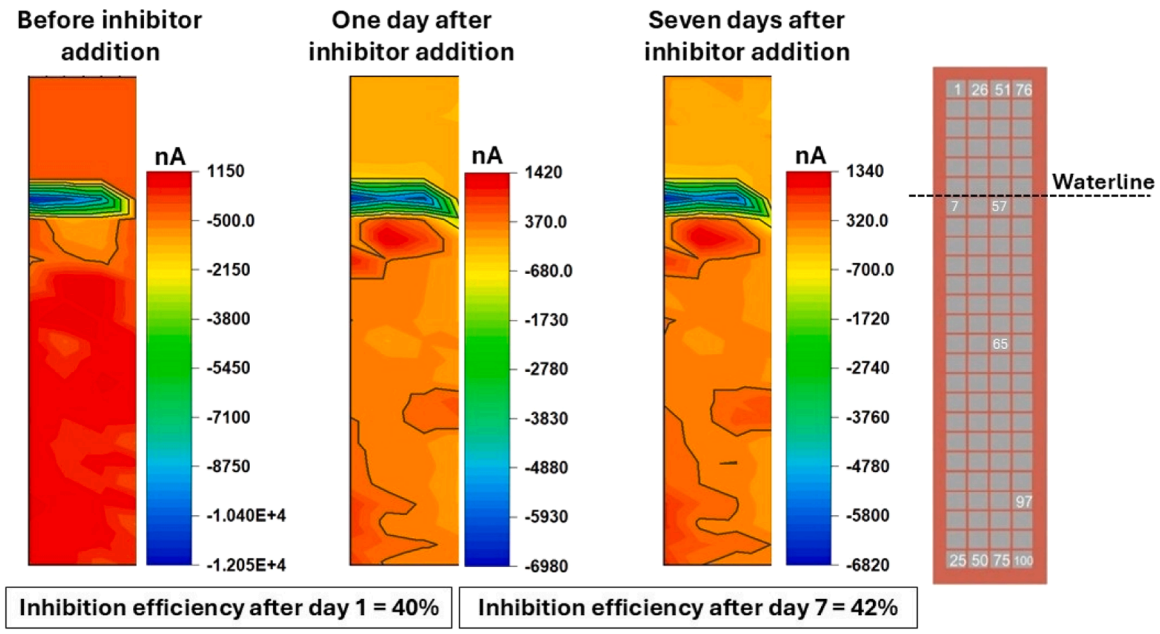

Fig. 7. Galvanic current distribution maps before, one day after, and seven days after adding $[Y_2(4hob)_6(H_2O)_4].2H_2O$ inhibitor to the 3.5 wt % NaCl solution. Note that before adding the inhibitor, the WBE probe was corroded for 14 days under the waterline corrosion conditions. Schematic illustration of the WBE probe is also presented to indicate the location of electrodes where the local potentiodynamic polarisations measurements are done.

and a Pt-coated Ti mesh was the counter electrode (58 mm × 10 mm). At local anodes, the potential was swept from 50 mV below the open circuit potential (OCP) to 300 mV above the OCP, and at local cathodes, the potential was swept from 300 mV below the OCP to 50 mV above the OCP at a scan rate of 1mV/sec. Each potential range was chosen carefully such that it was small enough to minimise any surface attack due to polarisation measurements, but large enough to show the electrochemical changes due to inhibitor additions. Local electrochemical impedance spectroscopy (EIS) measurements were performed at each individual electrode below the waterline, with a frequency range was from 10 mHz to 100 kHz using an AC perturbation of 10 mV. The EIS data were fitted to a simple electrical circuit based on what was observed on the surfaces. The circuit is discussed later in this paper. This allowed the film resistance and local EIS maps to be drawn for each local electrode below the waterline. Local EIS measurements were performed before the local polarisation measurements were obtained. A Bio-Logic VSP multi-channel potentiostat was used for all the electrochemical measurements and EC-Lab Software V11.36 was used for analysis. Further information on galvanic current mapping, local polarisation measurements and local EIS can be found in previous papers [1,42,44].

In addition to galvanic mapping, local polarisation and local EIS measurements were combined to estimate local metal loss. The local EIS fits provided the polarisation resistance, $R_p \approx (R_{ct} + R_f)$ (excluding R_s), while the local potentiodynamic curves yielded Tafel slopes (β_a and β_c) needed to determine the Stern-Geary constant using the following equation:

$$B = \frac{\beta_a \beta_c}{2.303\ (\beta_a + \beta_c)} \tag{2}$$

From these parameters, the local corrosion current density can be calculated using the Eq. (4) and then converted to a corrosion rate using Faraday's law (Eq. (5)).

$$i_{corr} = \frac{B}{R_p} \tag{3}$$

$$\mathrm{CR\ (mm/year)} = 0.00327 \times \mathrm{i_{corr}\ (\mu A.cm^{-2})} \times \frac{EW}{\rho} \tag{4}$$

Where EW is the equivalent weight for carbon steel (27) and ρ is the carbon steel density (~ 7.85 $g.cm^{-3}$). This approach allows quantitative estimation of metal dissolution rates at specific electrodes, complementing the qualitative insights from current distribution and film resistance maps.

3. Results and discussion

3.1. The behaviour of REM inhibitors in mitigating waterline corrosion on pre-rusted steel

Fig. 2 compares galvanic current distribution maps recorded before inhibitor addition, one day after addition, and seven days after addition. Before $La(4OHcin)_3{\cdot}5H_2O$ addition, a strong cathodic region (blueish colour) is clearly visible at and just above the waterline, with a peak cathodic current of approximately 11,860 nA, while anodic zones (reddish colour) below the waterline reach currents up to 2100 nA. This pattern reflects the classic differential aeration cell, with oxygen-rich areas acting as cathodes and oxygen-depleted, submerged areas as anodes [13–17]. One day after $La(4OHcin)_3{\cdot}5H_2O$ addition, the peak cathodic current drops sharply by ~71 % (from ~11,860 nA to ~3460 nA), and the blue cathodic footprint contracts noticeably. Anodic currents also reduced in several areas, though persistent hotspots particularly at corners of the probe remained unchanged. Seven days after $La(4OHcin)_3{\cdot}5H_2O$ addition, cathodic currents undergo only a marginal further decrease (to ~3280 nA), and the spatial distribution stabilises, indicating that the inhibitor's cathodic effect occurred rapidly and then plateaued. Anodic regions likewise show little additional suppression, confirming that $La(4OHcin)_3{\cdot}5H_2O$ alone could not fully overcome the barrier imposed by the rust. Overall, the inhibition efficiency calculated from the total anodic current was 42 % after one day and increased only to 49 % after seven days, substantially lower than the ≳90 % efficiency reported on fresh steel at the waterline [42]. These results clearly show that $La(4OHcin)_3{\cdot}5H_2O$ is ineffective in inhibiting waterline corrosion of pre-rusted steel surface and that the pre-rust layer significantly affected the inhibition efficiency.

To further understand the effects of REM inhibitors on the anodic and cathodic corrosion processes, local potentiodynamic polarisation

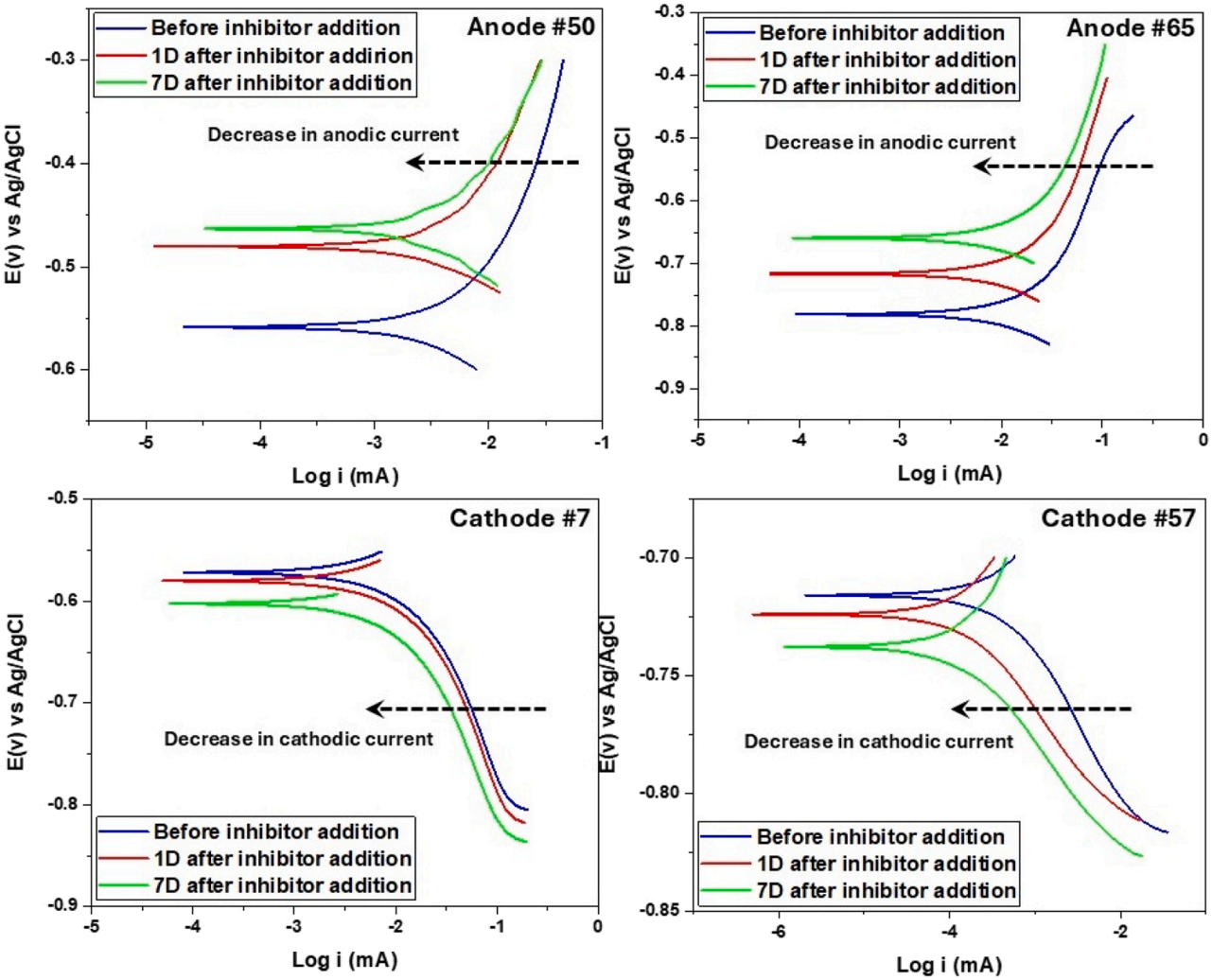

Fig. 8. Local potentiodynamic polarisation curves measured on the representative local anodic sites #50 and #65 and local cathodic sites #7 and #57 before, one day after, and seven days after addition of $[Y_2(4hob)_6(H_2O)_4].2H_2O$ inhibitor to 3.5 wt % NaCl solution. To see the location of the anodic and cathodic electrodes, please refer to the schematic of the WBE in Fig. 7.

measurements were conducted at local anodic and cathodic sites to understand the electrochemical changes at local areas. Fig. 3 presents potentiodynamic polarisation curves recorded at representative anodic sites (electrodes #50 and #65) and cathodic sites (electrodes #7 and #57) before inhibitor addition (blue curve), one day (red curve) and seven days (green curve) after inhibitor addition. One day after La $(4OHcin)_3{\cdot}5H_2O$ addition, the anodic current density at anodic sites #50 and #65 decreases, suggesting rapid adsorption of La-carboxylate ions that impede metal dissolution. Between day 1 and day 7, only marginal reduction in anodic current is observed, indicating that the initial protective film formed quickly but exhibited limited thickening or repair over longer exposures. On the other hand, at day 1, cathodic currents at cathodic sites #7 and #57 remain essentially unchanged, suggesting that hydroxide precipitation of La^{3+} was not yet complete. By day 7, cathodic currents show an obvious decrease, probably due to the gradual formation of a lanthanum hydroxide layer that hindered the oxygen reduction reaction. These observations confirm that $La(4OHcin)_3{\cdot}5H_2O$ acts as a mixed inhibitor. It rapidly adsorbs at anodic sites to suppress metal dissolution and more slowly precipitates at cathodic sites to impede oxygen reduction [27–29]. However, the pre-existing rust layer significantly limits inhibitor access, capping the overall inhibition efficiency at <50 % on pre-rusted steel.

Building on the protocol described above, another REM inhibitor [$Y(mbp)_3(H_2O)$] was introduced into a 3.5 wt % NaCl solution after a 14-day pre-rust period to assess its efficacy under identical conditions. The previous work showed that $[Y(mbp)_3(H_2O)]$ exhibited better inhibition efficiency than $La(4OHcin)_3{\cdot}5H_2O$ for localised corrosion on fresh steel (without rust) at the waterline [42]. Fig. 4 presents galvanic current distribution maps before, one day after, and seven days after $[Y(mbp)_3(H_2O)]$ addition. Before $[Y(mbp)_3(H_2O)]$ addition, the galvanic current distribution map mirrors the $La(4OHcin)_3{\cdot}5H_2O$ inhibitor baseline, with peak cathodic currents of ~11,140 nA and anodic hotspots up to ~1400 nA. One day after $[Y(mbp)_3(H_2O)]$ addition, the peak cathodic current decreased by ~79 % (to ~2250 nA), slightly higher than $La(4OHcin)_3{\cdot}5H_2O$ at day 1. Anodic currents also decline in several areas, though persistent hotspots particularly at corners of the probe remain unchanged, like the case of $La(4OHcin)_3{\cdot}5H_2O$ shown in Fig. 2. Seven days after $[Y(mbp)_3(H_2O)]$ addition, cathodic currents undergo only a marginal further decrease (to ~1990 nA), indicating that the inhibitor's cathodic effect occurred rapidly and then plateaued. Anodic regions, on the other hand, show little additional increase, confirming that $[Y(mbp)_3(H_2O)]$ could not fully overcome the barrier imposed by the rust. Overall, the inhibition efficiency calculated from the total anodic current is 41 % after one day and increases only to 46 % after seven days, substantially lower than the ≳90 % efficiency reported on fresh steel at the waterline [42]. These results clearly show that [Y

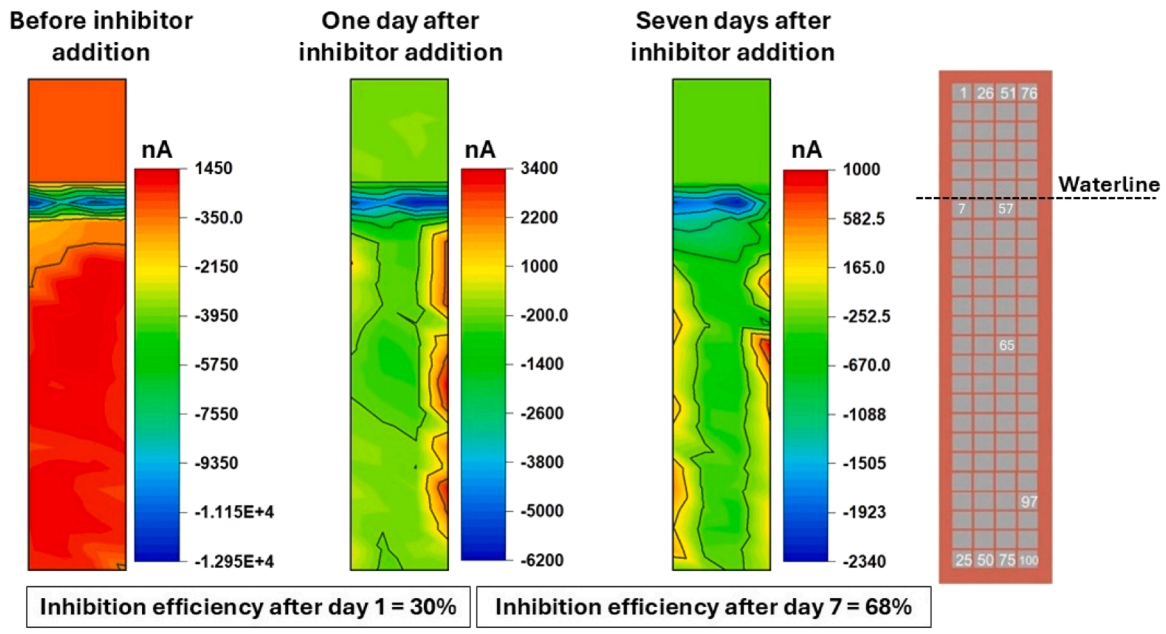

Fig. 9. Galvanic current distribution maps before, one day after, and seven days after adding mix inhibitor La(4OHcin)$_3$·5H$_2$O + sodium molybdate to the 3.5 wt % NaCl solution. Note that before adding the inhibitor, the WBE probe was corroded for 14 days under the waterline corrosion conditions. Schematic illustration of the WBE probe is also presented to indicate the location of electrodes where the local potentiodynamic polarisations measurements are done.

(mbp)$_3$(H$_2$O)] is ineffective in inhibiting waterline corrosion of pre-rusted steel surface and that the pre-rust layer significantly affected the inhibition efficiency. Fig. 5 presents potentiodynamic polarisation curves recorded at representative anodic sites (electrodes #50 and #65) and cathodic sites (electrodes #7 and #57) before [Y(mbp)$_3$(H$_2$O)] addition (blue curve), one day after (red curve), and seven days after (green curve). Generally, [Y(mbp)$_3$(H$_2$O)] addition results in almost similar behaviour compared to what was observed for La(4OHcin)$_3$·5H$_2$O addition in Fig. 3.

Forsyth et al. [30] suggested a mechanism to describe the inhibition of REM carboxylates. According to that mechanism, these are mixed inhibitors. At cathodic sites on a steel surface where an alkaline pH develops due to the oxygen reduction reaction, a precipitate of an REM hydroxide forms, which reduces the rate of the cathodic reaction. At anodic sites, carboxylate ions adhere to the steel surface by adsorption and form a protective film. Therefore, the rates of the anodic and cathodic reactions are reduced, hence the corrosion rate is reduced. The results above show that the inhibition efficiency of these two REM carboxylate inhibitors were significantly lower on pre-rusted steel with a rust layer present compared to the inhibition efficiencies on fresh steel (without rust). There may be two explanations for that: (i) the rust layer acts as a physical barrier and reduces the penetration ability of inhibitors through the rust layer into the steel surface; and (ii) REM carboxylate inhibitors become ineffective in the acidic environment which develops in the crevice between rust layer and steel surface with the extension of corrosion exposure [1]. Previously it was found that an acidic environment forms in between the rust layer and the steel surface leading to crevice corrosion [1–4]. REM carboxylates are unable to mitigate the crevice corrosion as shown by their low inhibition efficiency when rust is present on the steel surface, compared to their inhibition efficiency with fresh steel samples.

To probe whether a smaller REM carboxylate molecule could better penetrate the rust layer, [Y$_2$(4hob)$_6$(H$_2$O)$_4$].2H$_2$O was tested, which features a shorter carboxylate chain [43,45,48] than both La(4OHcin)$_3$·5H$_2$O and [Y(mbp)$_3$(H$_2$O)] (chemical structure shown in Fig. 6). Fig. 7a–c presents galvanic current distribution maps recorded before, one day after, and seven days after adding [Y$_2$(4hob)$_6$(H$_2$O)$_4$].2H$_2$O. Despite its smaller size, this inhibitor produced virtually the same cathodic footprint at the waterline and anodic hotspots below as the larger REM carboxylates, yielding overall inhibition efficiencies of 40 % and 42 % at days 1 and 7, respectively.

Local polarisation measurements shown in Fig. 8, indicate that [Y$_2$(4hob)$_6$(H$_2$O)$_4$].2H$_2$O decreases the anodic kinetics at local anodes and cathodic kinetics at local cathodes which is similar to the effects of La(4OHcin)$_3$·5H$_2$O and [Y(mbp)$_3$(H$_2$O)]. These results suggest that the attempt to enhancing the inhibition efficiency through changing the rare earth elements and molecular size was not successful.

3.2. *The behaviour of REM-inorganic mixed inhibitors in mitigating waterline corrosion on pre-rusted steel*

To enhance the performance of REM carboxylates on inhibiting corrosion of pre-rusted steel, binary mixtures of La(4OHcin)$_3$·5H$_2$O or [Y(mbp)$_3$(H$_2$O)] with sodium molybdate were evaluated. Sodium molybdate is known both to buffer local acidity and to promote formation of compact, Mo-rich passive films at anodic sites [46,47]. Figs. 9–12 track how these mix inhibitors affect the corrosion processes. As shown in Fig. 9, the mixed inhibitor La(4OHcin)$_3$·5H$_2$O + sodium molybdate shows an inhibition efficiency of 68 % after seven days of inhibitor addition. This is a significant increase compared to the inhibition efficiency of La(4OHcin)$_3$·5H$_2$O that showed 49 % inhibition efficiency seven days after the inhibitor addition (Fig. 2). As shown in Fig. 9, there were several major anodic sites seven days after adding the mix inhibitor, however the peak anodic current at those areas decreased from 1450 nA to 1000 nA. Furthermore, after adding the mixed inhibitor, there is a significant decrease in cathodic current at the waterline where the major cathodic site is present. According to the local polarisation measurements shown in Fig. 10, the inhibitor mixture caused a significant decrease in anodic kinetics at local anodic sites not only after one day of inhibitor addition but also after seven days of inhibitor addition. This is an improvement compared to La(4OHcin)$_3$·5H$_2$O itself as there was little or no decrease in anodic kinetics after seven days of La(4OHcin)$_3$·5H$_2$O addition compared to one day after the inhibitor addition (Fig. 3). Furthermore, there is a larger decrease in anodic kinetics seven days after adding the inhibitor mixture compared to La(4OHcin)$_3$·5H$_2$O. The effects of the mixed inhibitor on cathodic kinetics

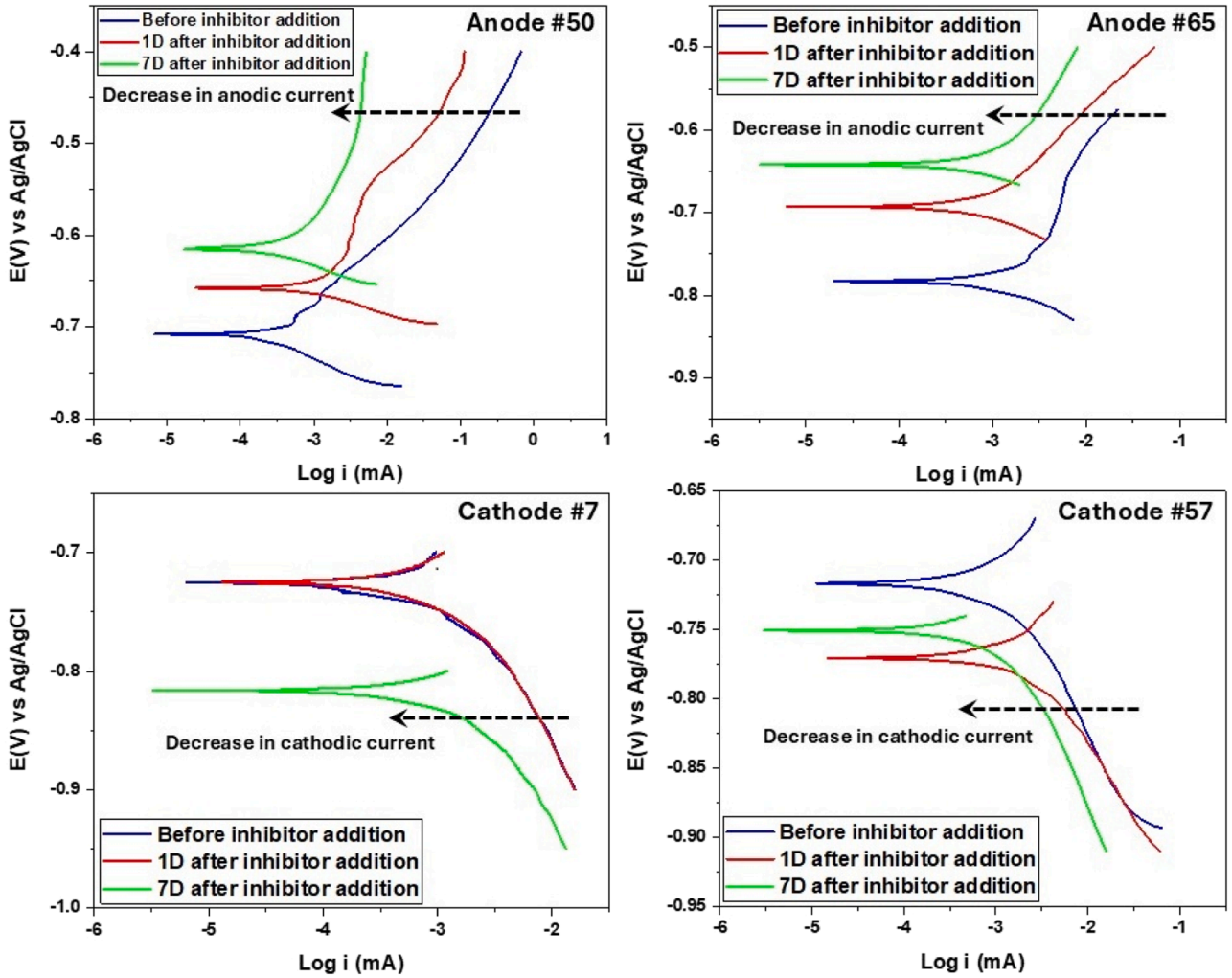

Fig. 10. Local potentiodynamic polarisation curves measured on the representative local anodic sites #50 and #65 and local cathodic sites #7 and #57 before, one day after, and seven days after addition of mix inhibitor La(4OHcin)$_3$·5H$_2$O + sodium molybdate to 3.5 wt % NaCl solution. To see the location of the anodic and cathodic electrodes, please refer to the schematic of the WBE in Fig. 9.

is similar to La(4OHcin)$_3$·5H$_2$O itself. After one day of the inhibitor addition, there is little or no change, while there is a significant decrease in cathodic kinetics seven days after adding the inhibitor mixture.

Further experiments have been conducted to evaluate the efficiency of mixed inhibitor of [Y(mbp)$_3$(H$_2$O)] + sodium molybdate. As shown in Fig. 11, the mixed inhibitor [Y(mbp)$_3$(H$_2$O)] + sodium molybdate showed 69 % inhibition efficiency seven days after adding the mixed inhibitor. These results further confirm that the inhibition efficiency of REM carboxylates can be increased significantly by mixing with the inorganic inhibitor sodium molybdate. When the current distribution maps are considered, it is clear that there are some major anodic sites remaining after adding the mixed inhibitor, as shown in Fig. 11, however, the anodic current values at those areas decreased significantly from 1650 nA to 1100 nA seven days after adding the mixed inhibitor. Furthermore, there is a significant decrease in cathodic current after adding the mixed inhibitor. As shown in Fig. 12, the inhibitor mixture caused a significant decrease in anodic kinetics at local anodic sites. Furthermore, it resulted in a decrease in the cathodic kinetics at local cathodic sites seven days after adding the inhibitor mixture.

3.3. Understanding the inhibition mechanisms of mixed inhibitors

To identify how mixing sodium molybdate with REM carboxylates boosts overall inhibition efficiency, it was evaluated the contribution of molybdate alone first, a species not previously tested for waterline corrosion on pre-rusted steel. As shown in Fig. 13, sodium molybdate by itself delivers only modest inhibition efficiencies of 38 % after one day and 50 % after seven days. Although several anodic hotspots remain, peak anodic currents fall from approximately 1650 nA to 1220 nA over the course of a week.

Local potentiodynamic polarisation curves (Fig. 14) reveal that molybdate selectively suppresses anodic kinetics; current densities at active anodes drop noticeably upon addition, whereas cathodic sites show negligible change. This behaviour confirms that sodium molybdate functions strictly as an anodic inhibitor. In accord with the literature [46,47], molybdate ions are known to form a compact passive film at anodic regions and to buffer local acidity via the reaction below [46, 49]:

$$MoO_4^{2-}{}_{(aq)} + 4H^+{}_{(aq)} + 2e^- -> MoO_{2(s)} + 2H_2O_{(l)} \quad (5)$$

By pairing this passive film enhancement and buffering action with the dual anodic + cathodic inhibition afforded by REM inhibitors, the mixed inhibitor achieves substantially higher inhibition efficiencies compared to either component alone.

If the local polarisation results from Figs. 10 and 12 are summarised, the mixed inhibitors exhibit the greatest reduction in anodic kinetics, achieving the highest seven-day inhibition efficiencies compared to each component alone. This confirms that mixed inhibitors suppress

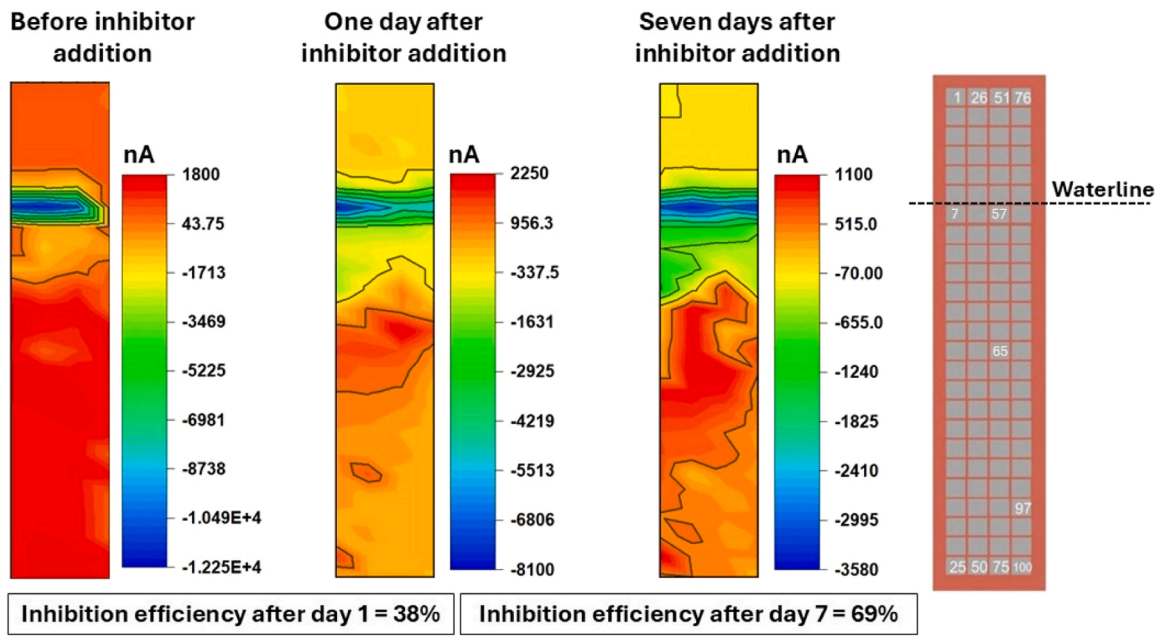

Fig. 11. Galvanic current distribution maps before, one day after, and seven days after adding mix inhibitor [Y(mbp)$_3$(H$_2$O)] + sodium molybdate to the 3.5 wt % NaCl solution. Note that before adding the inhibitor, the WBE probe was corroded for 14 days under the waterline corrosion conditions. Schematic illustration of the WBE probe is also presented to indicate the location of electrodes where the local potentiodynamic polarisations measurements are done.

corrosion at anodic sites more effectively. Several factors contribute to this enhanced anodic inhibition: (i) REM carboxylates adsorb onto anodic sites and form a protective film, immediately reducing metal dissolution; (ii) Sodium molybdate promotes passive film formation by precipitating molybdenum oxides/hydroxides and buffering acidic microenvironments. Together, these actions produce a pronounced decrease in anodic currents when both inhibitors are present, supporting the hypothesis that molybdate enhances anodic inhibition through both pH buffering and passive film formation [46,47]. The result is a clear synergistic effect between organic REM complexes and the inorganic sodium molybdate.

After adding REM carboxylate inhibitors alone, cathodic kinetics remain unchanged at 24 h but drop significantly by day 7. According to Forsyth et al., REM ions slowly precipitate as hydroxides at cathodic sites under alkaline conditions [30], accounting for the delayed cathodic suppression. Mixed inhibitors follow the same trend, since they contain REM carboxylates, whereas sodium molybdate on its own induces no cathodic effect, consistent with its strict anodic-only behaviour [46,47].

Collectively, local polarisation curves in Figs. 3, 5, 8, 10, and 12 show that at anodic sites, the OCP values generally shifted in a more positive direction when inhibitors were present. Such positive OCP shifts generally reflect reduced anodic metal dissolution activities, which is particularly pronounced when rare-earth and molybdate inhibitors are used together. This is consistent with adsorption of rare-earth carboxylates and the stabilising and protective effects of molybdate-assisted passive films.

To further elucidate site-specific film formation, local EIS measurements across the corroded WBE probe were employed. Fig. 15a presents photographs of the probe surface after seven days of exposure (following a 14-day pre-corrosion), alongside EIS distribution maps based on fitted film-resistance values. Notably, only REM-containing solutions yield a white deposit at and just below the waterline, identified by FTIR in the previous work (broad OH stretching band near 3000 cm^{-1}) as lanthanide hydroxide (La(OH)$_3$ or Y(OH)$_3$) [42]. The absence of this deposit for molybdate alone confirms its anodic-only action.

The EIS maps in Fig. 15c reveal that, below the waterline, REM and mixed inhibitors form uniform, high-resistance films, whereas molybdate alone produces comparatively low resistance at cathodic regions, underscoring its inability to protect cathodes. Peak film resistances for La(4OHcin)$_3$·5H$_2$O, [Y(mbp)$_3$(H$_2$O)], and sodium molybdate are approximately 9 kΩ, 10 kΩ, and 8 kΩ, respectively. In contrast, the La–molybdate and Y–molybdate mixtures reach ~25 kΩ and ~28 kΩ, demonstrating that molybdate markedly strengthens the mixed inhibitor film.

All EIS data were fitted using the equivalent-circuit in Fig. 15b (adapted from Nam et al. [50] and Peng et al. [51]): R_s the solution resistance; R_{ct} the charge-transfer resistance; R_f, the combined rust and inhibitor-film resistance; CPE_f the film capacitance (constant phase element); and CPE_d, the double-layer capacitance. The use of CPE accounts for non-ideal behaviour arising from rust and inhibitor film heterogeneity [52]. Local EIS thus proves invaluable for mapping protective film properties at distinct anodic and cathodic sites, insights unattainable via global EIS alone. Likewise, local polarisation measurements precisely reveal the differential effects of anodic-only versus dual-action inhibitors on site-specific kinetics.

While the EIS maps provide valuable information on film resistance distribution, they do not directly convey the extent of metal loss due to corrosion. To better quantify the corrosion severity under different conditions and the performance of each inhibitor in reducing the corrosion metal loss, the impedance data were further processed to estimate local corrosion current densities and corresponding metal dissolution rates according to the procedure described in the Materials and Methods (Section 2). Results are summarised in Table 1.

The quantitative estimation of metal dissolution rates derived from local EIS and polarisation data (Table 1) further highlights the critical influence of inhibitor chemistry on inhibition performance, hence the metal loss. For single-component inhibitors, corrosion rates remained relatively high, with La(4OHcin)$_3$·5H$_2$O and [Y(mbp)$_3$(H$_2$O)] yielding 1.59 and 0.77 μm/year, respectively, while sodium molybdate alone produced a comparable value of 1.42 μm/year. These results confirm that neither REM carboxylates nor molybdate individually can adequately suppress metal loss on pre-rusted steel, as the barrier imposed by the rust layer limits their effectiveness. In contrast, mixed inhibitor systems achieved a dramatic reduction in corrosion rate, with La(4OHcin)$_3$·5H$_2$O + molybdate and [Y(mbp)$_3$(H$_2$O)] + molybdate lowering values to 0.38 and 0.26 μm/year, respectively, representing

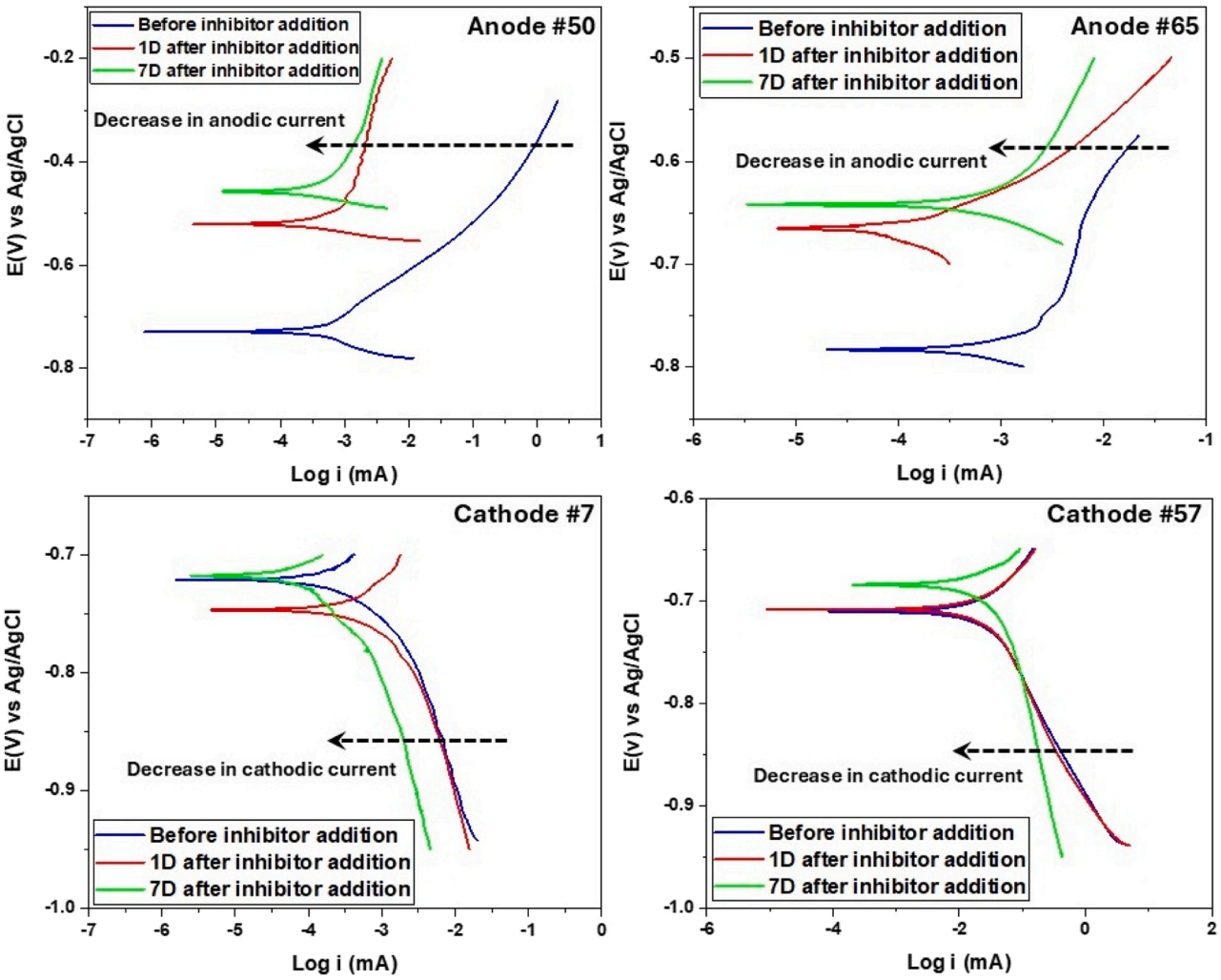

Fig. 12. Local potentiodynamic polarisation curves measured on the representative local anodic sites #50 and #65 and local cathodic sites #7 and #57 before, one day after, and seven days after addition of mix inhibitor [$Y(mbp)_3(H_2O)$] + sodium molybdate to 3.5 wt % NaCl solution. To see the location of the anodic and cathodic electrodes, please refer to the schematic of the WBE in Fig. 11.

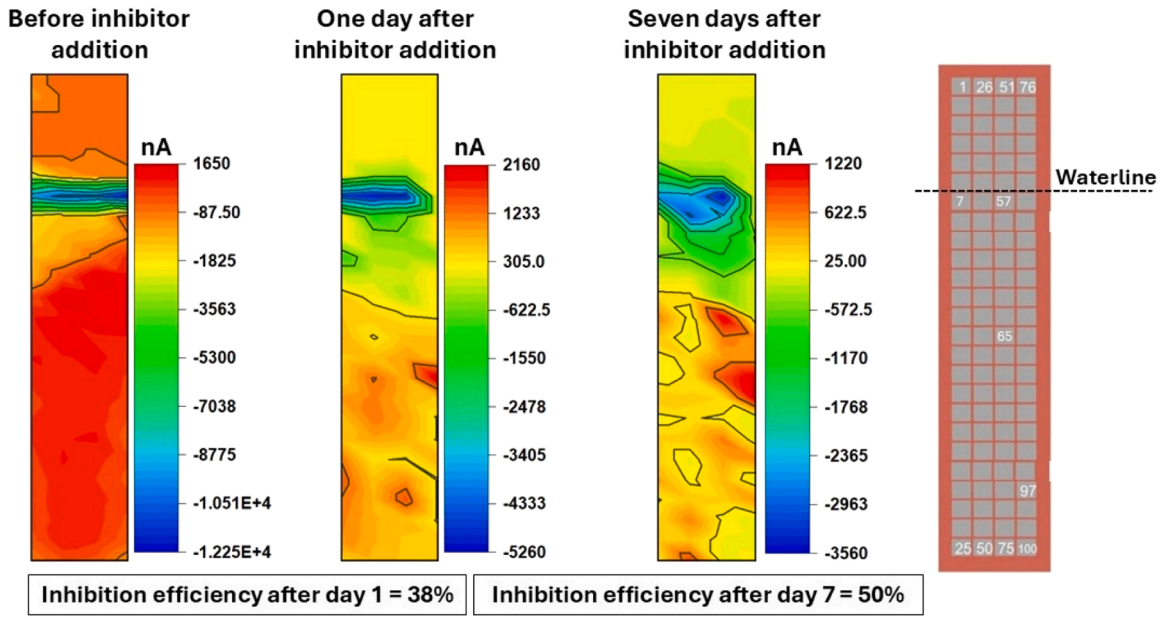

Fig. 13. Galvanic current distribution maps before, one day after, and seven days after adding sodium molybdate to the 3.5 wt % NaCl solution. Note that before adding the inhibitor, the WBE probe was corroded for 14 days under the waterline corrosion conditions. Schematic illustration of the WBE probe is also presented to indicate the location of electrodes where the local potentiodynamic polarisations measurements are done.

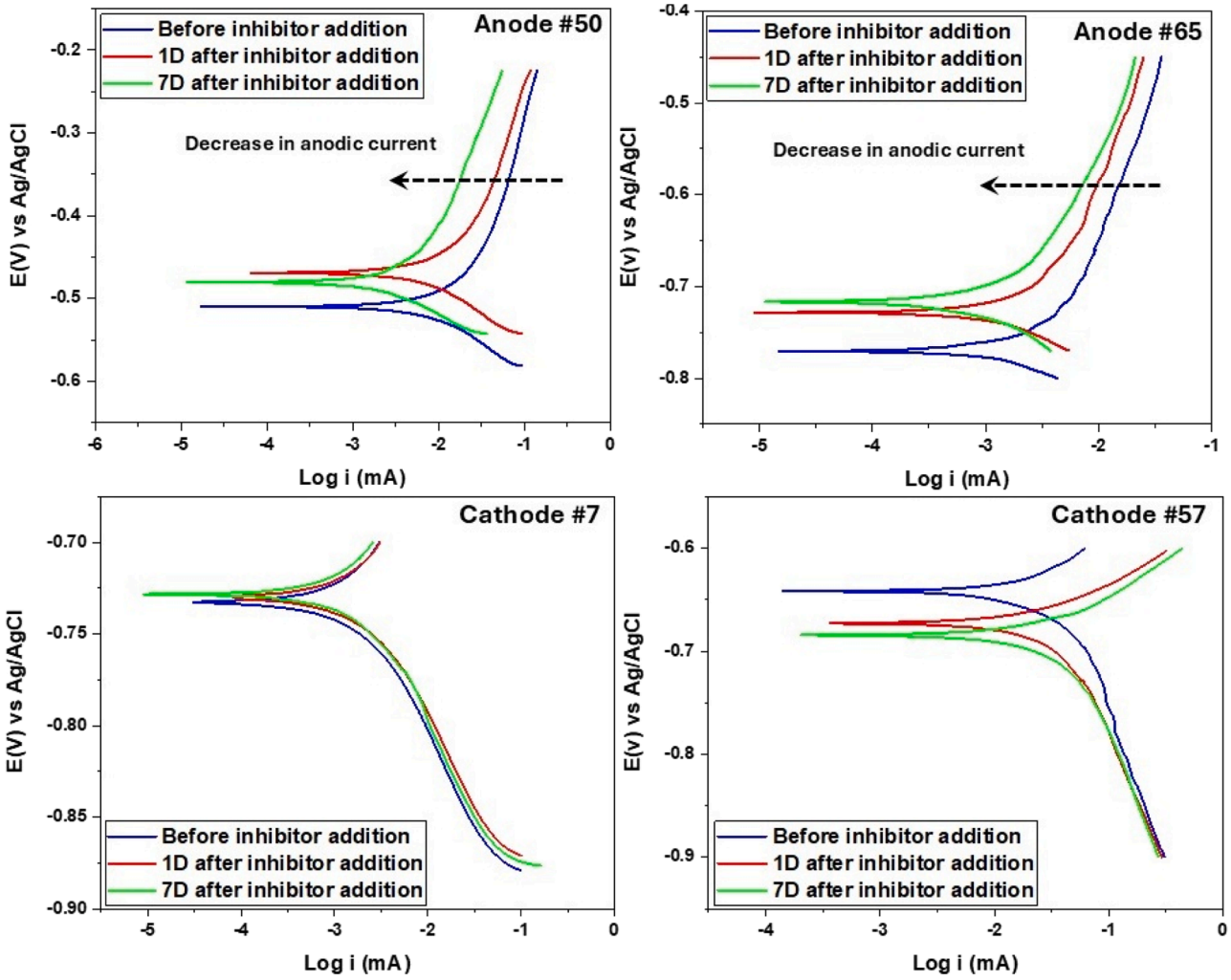

Fig. 14. Local potentiodynamic polarisation curves measured on the representative local anodic sites #50 and #65 and local cathodic sites #7 and #57 before, one day after, and seven days after addition of sodium molybdate to 3.5 wt % NaCl solution. To see the location of the anodic and cathodic electrodes, please refer to the schematic of the WBE in Fig. 13.

more than a four- to six-fold improvement compared to the single-inhibitor cases. This reduction in metal loss correlates strongly with the significantly higher film resistances observed for the mixed systems, confirming that the synergistic action of REM adsorption and molybdate-assisted passive film formation results in more robust and protective surface layers. These findings not only validate the synergistic mechanism proposed but also demonstrate that effective mitigation of waterline corrosion on pre-rusted steel requires such hybrid inhibitor systems to meaningfully reduce long-term structural degradation. This hybrid organic–inorganic approach represents a promising strategy for mitigating localised corrosion on aging marine and industrial steel infrastructure. Future work should explore the long-term stability of these mixed films under cyclic wet-dry conditions and evaluate environmental compatibility in real-world deployment.

4. Conclusions

This study assesses the performance of three REM inhibitors, i.e., La(4OHcin)$_3$·5H$_2$O, [Y(mbp)$_3$(H$_2$O)], and [Y$_2$(4hob)$_6$(H$_2$O)$_4$].2H$_2$O against waterline corrosion on pre-rusted steel, and to test whether mixing these organic inhibitors with the inorganic anodic inhibitor sodium molybdate could overcome the barrier imposed by existing rust layers. Using a WBE probe, *in-situ* galvanic current mapping, local potentiodynamic polarisation, and local EIS measurements were employed to monitor both kinetics and protective film development at discrete anodic and cathodic sites. Key findings can be summarised as follows:

1. All three REM inhibitors achieved only 40–49 % inhibition efficiencies after seven days on pre-rusted steel, which are substantially lower than the ≳90 % efficiencies previously reported on fresh (unrusted) steel. Galvanic current distribution maps showed persistent anodic "hotspots" and only marginal additional suppression beyond the first 24 h, indicating that the rust layer acts as a physical and chemical barrier to both inhibitor adsorption and hydroxide precipitation at cathodic sites.
2. Sodium molybdate yielded inhibition efficiencies of 38 % after one day and 50 % after seven days. Local polarisation curves confirmed that molybdate selectively suppresses anodic kinetics by promoting passive film formation and buffering local acidity, but it offers no cathodic protection.
3. Combining REM inhibitors with sodium molybdate boosted inhibition efficiencies to 68 % (La–molybdate) and 69 % (Y–molybdate) after seven days, over 20 % higher than REM alone. Mixed inhibitors produced more uniform, high-resistance films (25–28 kΩ) across the WBE, compared to 8–10 kΩ for single-inhibitor systems. Local potentiodynamic polarisation measurements revealed pronounced anodic suppression that continued to develop over a week, while

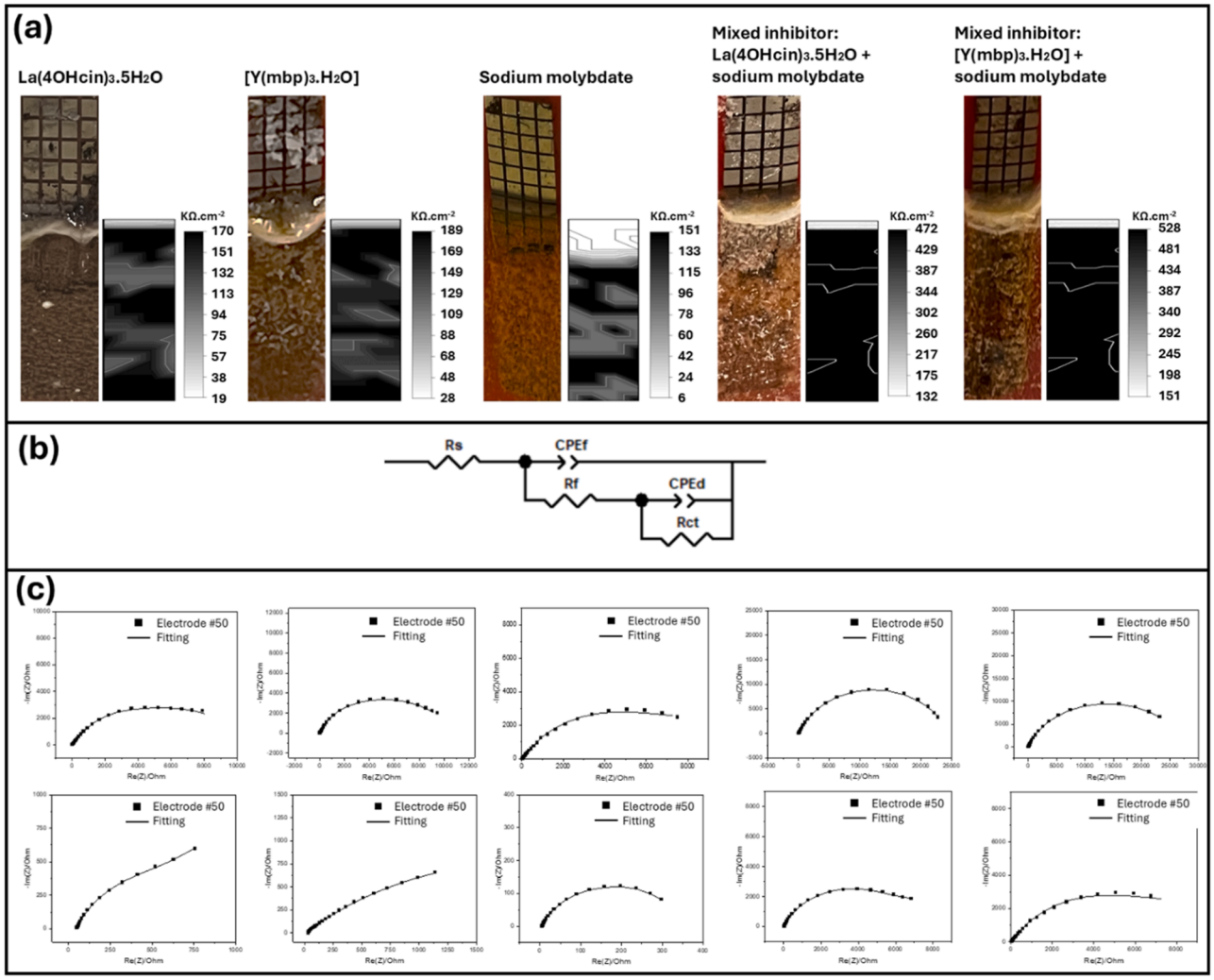

Fig. 15. (a) Photographs of the WBE probe after 7 days of exposure to solutions containing La(4OHcin)$_3$·5H$_2$O, [Y(mbp)$_3$(H$_2$O)], sodium molybdate, mixture (La(4OHcin)$_3$·5H$_2$O + sodium molybdate) and mixture ([Y(mbp)$_3$(H$_2$O)] + sodium molybdate) alongside EIS distribution maps which are drawn using the film resistance values from the fitted graph at each electrode. Note that before adding the inhibitor, the WBE probe was corroded for 14 days under the waterline corrosion conditions. (b) The equivalent circuit model used to fit EIS data. (c) Representative local Nyquist plots and fittings obtained at local areas of the probe surface.

Table 1
Summary of electrochemical parameters obtained from local EIS fittings and potentiodynamic polarisation measurements on pre-rusted steel after 7 days of inhibitor exposure in 3.5 wt % NaCl solution.

Condition	R_{ct} (Ω/cm^2)	R_f (Ω/cm^2)	R_p (Ω/cm^2)	β_a (V/decade)	β_c (V/decade)	B	i_{corr} (μA/cm^2)	CR (mm/year)	CR (μm/year)
La(4OHcin)$_3$·5H$_2$O	4800	143,200	148,000	0.1991	0.0636	0.02093	0.1414	0.00159	1.59
[Y(mbp)$_3$(H$_2$O)]	4900	160,500	165,400	0.1441	0.0320	0.01137	0.0687	0.00077	0.77
Sodium molybdate	5800	128,600	134,400	0.1313	0.0557	0.01698	0.1264	0.00142	1.42
La(4OHcin)$_3$·5H$_2$O + sodium molybdate	4200	452,000	456,200	0.1907	0.0455	0.01567	0.0343	0.00039	0.38
[Y(mbp)$_3$(H$_2$O)] + sodium molybdate	4400	506,200	510,600	0.1633	0.0328	0.01168	0.0232	0.00026	0.26

cathodic kinetics were progressively hindered by REM hydroxide precipitation.

CRediT authorship contribution statement

Medhani Pathirana: Writing – review & editing, Writing – original draft, Visualization, Validation, Methodology, Investigation, Formal analysis, Data curation, Conceptualization. **Majid Laleh:** Writing – review & editing, Visualization, Validation, Supervision, Methodology, Investigation, Formal analysis, Data curation. **Anthony Somers:** Writing – review & editing, Validation, Supervision, Resources, Methodology, Formal analysis. **Bruce Hinton:** Writing – review & editing, Validation, Supervision, Formal analysis. **Glen B. Deacon:** Writing – review & editing, Validation, Supervision, Resources, Funding acquisition, Formal analysis. **Peter C. Junk:** Writing – review & editing, Validation, Supervision, Project administration, Funding acquisition,

Formal analysis. **Mike Yongjun Tan:** Writing – review & editing, Visualization, Validation, Supervision, Resources, Project administration, Methodology, Investigation, Funding acquisition, Formal analysis, Conceptualization.

Declaration of competing interest

The authors declare that they have no known competing financial interests or personal relationships that could have appeared to influence the work reported in this paper.

Acknowledgements

Financial support from Australian Research Council funding for ARC Discovery project ID: DP200100568 is gratefully acknowledged.

Data availability

The raw/processed data required to reproduce these findings cannot be shared at this time as the data also forms part of an ongoing study.

References

[1] M. Pathirana, M. Laleh, A. Somers, B. Hinton, M.Y. Tan, The critical effect of rust layers on localised corrosion of steel exposed to waterline environments, Corros. Sci. 221 (2023) 111333.
[2] X. Li, F. Gui, H. Cong, C. Brossia, G. Frankel, Examination of mechanisms for liquid-air-interface corrosion of steel in high level radioactive waste simulants, J. Electrochem. Soc. 160 (11) (2013) C521.
[3] G. Frankel, Pitting corrosion of metals a review of the critical factors, J. Electrochem. Soc. 145 (6) (1998) 2186–2198.
[4] N. Laycock, J. Stewart, R. Newman, The initiation of crevice corrosion in stainless steels, Corros. Sci. 39 (10–11) (1997) 1791–1809.
[5] M. Peterson, L.J. Waldron, Investigation of mild steel corrosion rate in San Diego harbor, Corrosion 17 (4) (1961), 188t–190t.
[6] J.A. Beavers, N. Sridhar, K.D. Boomer, Corrosion management of the Hanford high-level nuclear waste tanks, JOM 66 (3) (2014) 491–502.
[7] X. Li, F. Gui, H. Cong, C. Brossia, G. Frankel, Examination of mechanisms for liquid-air-interface corrosion of steel in high level radioactive waste simulants, J. Electrochem. Soc. 160 (11) (2013) C521.
[8] B. Piri, R. Amini, E. Asadinia, S. Vardak, R. Mehdilouee, A. Mojarrad, Investigation of failure mechanisms and remaining life prediction of firewater pipelines used in industrial applications, Eng. Fail. Anal. 124 (2021) 105301.
[9] R. Ray, J. Lee, B. Little, Factors contributing to corrosion of steel pilings in Duluth-Superior Harbor, Corrosion 65 (11) (2009) 707–717.
[10] M. Laleh, Y. Huo, M.B. Kannan, R.B. Petersen, R.E. Melchers, M.Y. Tan, Probing and monitoring multiple forms of localised corrosion occurring concurrently on pipeline steels in marine environments, Corros. Sci. 214 (2024) 112453.
[11] M. Laleh, Y. Huo, R.E. Melchers, M.Y. Tan, Electrode array probe designed for visualising and monitoring multiple localised corrosion processes and mechanisms simultaneously occurring on marine structures, NPJ Mater. Degradat. 7 (2023) 68.
[12] U. Evans, Report on corrosion research work at Cambridge University, Inter. Outbreak War, J. Iron Steel Inst. 141 (1940) 219–234.
[13] J. De Gruyter, S. Mertens, E. Temmerman, Corrosion due to differential aeration reconsidered, J. Electroanal. Chem. 506 (1) (2001) 61–63.
[14] Y. Tan, Monitoring localized corrosion processes and estimating localized corrosion rates using a wire-beam electrode, Corrosion 54 (5) (1998) 403–413.
[15] E. McCafferty, Introduction to Corrosion Science, Springer Science & Business Media, New York, 2010.
[16] R.W. Revie, Corrosion and Corrosion Control: An Introduction to Corrosion Science and Engineering. & Sons, John Wiley, 2008.
[17] Y. Chen, W. Zhang, J. Ding, P. Yin, J. Wang, Y. Zou, Research on water-line corrosion of carbon steel by wire beam electrode technique, MATEC Web Conf. EDP Sci. (2016) 01004.
[18] R.E. Melchers, R. Jeffrey, Corrosion of long vertical steel strips in the marine tidal zone and implications for ALWC, Corros. Sci. 65 (2012) 26–36.
[19] D. Peichang, L. Quanbing, L. Ziyun, W. Gui, H. Jiezhen, W. Xie, Corrosion behavior of X70 pipeline steel in the tropical juncture area of seawater-sea mud, J. Chin. Soc. Corros. Prot. 38 (5) (2018) 415–423.
[20] C. Li, L. Zhang, Z. Lu, R. Ding, X. Zhao, B. Wang, H. Cui, J. Liu, Studies on waterline corrosion processes and corrosion product characteristics of carbon steel in 3.5 wt % NaCl solution, Mater. Corros. 72 (4) (2021) 732–742.
[21] J. Wu, P. Wang, J. Gao, F. Tan, D. Zhang, Y. Cheng, S. Chen, Comparison of waterline corrosion processes in natural and artificial seawater: the role of microbes, Electrochem. Commun. 80 (2017) 9–15.
[22] R. Jeffrey, R.E. Melchers, Corrosion of vertical mild steel strips in seawater, Corros. Sci. 51 (10) (2009) 2291–2297.
[23] X. Li, F. Gui, H. Cong, C. Brossia, G. Frankel, Evaluation of nitrate and nitrite reduction kinetics related to liquid-air-interface corrosion, Electrochim. Acta 117 (2014) 299–309.
[24] Y. Xu, Y. Tan, Y. Huang, The study of water-line corrosion in static and dynamically flowing electrolytes using multi-electrode sensor in combination with electrical resistance method, corrosion & prevention 2018, in: Proc. Corros. Prev. Conf., Australas. Corros. Assoc, 2018, pp. 1–9.
[25] M.Y. Tan, S. Bailey, B. Kinsella, Mapping non-uniform corrosion using the wire beam electrode method. III. Water-line corrosion, Corros. Sci. 43 (10) (2001) 1931–1937.
[26] X. Li, H. Cong, F. Gui, C. Brossia, G. Frankel, Development of liquid-air-interface corrosion of steel in nitrate solutions, Corrosion 70 (3) (2014) 230–246.
[27] B.R.W. Hinton, P.N. Trathen, L. Wilson, The inhibition of mild steel corrosion in tap water by cerous chloride, in: 28th Annual Conference of Australasian Corrosion Association, Australasian Corrosion Association, Perth, Australia, 1988.
[28] B.R.W. Hinton, New Approaches to Corrosion Inhibition With Rare Earth Metal Salts, 89, NACE, New Orleans, 1989. CorrosionPaper No. 170.
[29] A.D. Mercer, The properties of carboxylates as corrosion inhibitors, in: Proc 5th European Symposium on Corrosion Inhibitors, Ferrara, Italy, 1980, pp. 563–581.
[30] M. Forsyth, M. Seter, B. Hinton, G. Deacon, P. Junk, New 'green' corrosion inhibitors based on rare earth compounds, Aust. J. Chem. 64 (2011) 812–819.
[31] F.J. Blin, S. Leary, K.E. Wilson, M. Forsyth, Evaluation of the Corrosion Mitigation Potential of Some New Rare Earth Metal Based Compounds On Steel, 02, Australasian Corrosion Association, CorrosionPaper, Adelaide, 2002, p. 79.
[32] F.J. Blin, S. Leary, K.E. Wilson, The inhibition of corrosion on mild steel with rare earth cinnamate compounds. Corrosion Control and NDT, Australasian Corrosion Association, Melbourne, 2003, p. 80, 2003.
[33] F. Blin, P. Koutsoukos, P. Klepetsianis, The corrosion inhibition mechanism of new rare earth cinnamate compounds – Electrochemical studies, Electrochim. Acta 52 (21) (2007) 6212–6220.
[34] M. Behrouzvaziri, The Effect of Concentration and Structure on La and Ce based Inhibitors On the Corrosion Rate of Mild Steel in Chloride Solution, Monash University MEngSc Thesis, Melbourne, 2009.
[35] M. Behrouzvaziri, B.R.W. Hinton, M. Forsyth, The effect of concentration and structure on La and Ce based inhibitors on the corrosion rate of mild steel in chloride solution, Corros. Prevent. (2008). Nov 2008.
[36] F. Blin, S.G. Leary, K. Wilson, Corrosion mitigation of mild steel by new rare earth cinnamate compounds, J. Appl. Electrochem. (2004) 591–599.
[37] J. Li, B. Hurley, R. Buchheit, Microelectrochemical characterization of the effect of rare earth inhibitors on the localized corrosion of AA2024-T3, J. Electrochem. Soc. 162 (10) (2015) C563–C571, https://doi.org/10.1149/2.0791510jes.
[38] G.B. Deacon, P.C. Junk, W.W. Lee, M. Forsyth, J. Wang, Rare earth 3-(4′-hydroxyphenyl) propionate complexes, New J. Chem. 39 (2015) 7688–7695.
[39] C.N. de Bruin-Dickason, G.B. Deacon, C.M. Forsyth, S. Hanf, O.B. Heilmann, B.R. W. Hinton, P.C. Junk, A.E. Somers, Y.Q. Tan, D.R. Turner, Synthesis and structures of rare earth 3-(4′-methylbenzoyl)-propanoate complexes-new corrosion inhibitors, Aust. J. Chem. 70 (2017) 478–484.
[40] M. Frey, S.G. Harris, J.M. Holmes, D.A. Nation, S. Parsons, P.A. Tasker, S.J. Teat, R. E. Winpenny, Modeling surface engineering: use of polymetallic iron cages and computer graphics to understand the mode of action of a corrosion inhibitor, Angew. Chem. Int. Ed. 37 (1998) 3245–3248.
[41] M. Frey, S.G. Harris, J.M. Holmes, D.A. Nation, S. Parsons, P.A. Tasker, R. E. Winpenny, Elucidating the mode of action of a corrosion inhibitor for iron, Chem. Eur. J. 6 (2000) 1407–1415.
[42] M. Pathirana, M. Laleh, A. Somers, B. Hinton, G.B. Deacon, P.C. Junk, M.Y. Tan, Exploring environmentally friendly localised corrosion inhibitors through local electrochemical measurements using multielectrode arrays, Electrochim. Acta 528 (2025), https://doi.org/10.1016/j.electacta.2025.146307.
[43] J. Moon, Z. Guo, O.A. Beaumont, S. Hamilton, G. Bousrez, E. Mottram, J. Wang, A. E. Somers, G.B. Deacon, P.C. Junk, 4-Hydroxybenzoato-rare earth(iii) complexes – syntheses, a structural goldmine from coordination diversity and improved corrosion inhibition behaviour, New J. Chem. 47 (36) (2023) 16843–16854, https://doi.org/10.1039/d3nj02735j.
[44] M. Laleh, M. Pathirana, M.Y. Tan, Site-specific local polarisation curve measurements for probing localised corrosion and inhibition, Corros. Sci. 214 (2023) 111019.
[45] G.B. Deacon, M. Forsyth, P.C. Junk, S.G. Leary, W.W. Lee, Synthesis and characterisation of rare earth complexes supported by para-substituted cinnamate ligands, Zeitschrift für Anorganische und Allgemeine Chemie 635 (6–7) (2009) 833–839, https://doi.org/10.1002/zaac.200801379.
[46] S.A.M. Refaey, S.S. Abd El-Rehim, F. Taha, M.B. Saleh, R.A. Ahmed, Inhibition of chloride localized corrosion of mild steel by PO_4^{3-}, CrO_4^{2-}, MoO_4^{2-}, and NO_2^- anions, Appl. Surf. Sci. 158 (2000) 190–196.
[47] Y.T. Tan, S.L. Wijesinghe, D.J. Blackwood, Effect of molybdate on the passivation of carbon steel in alkaline solutions under open-circuit conditions, J. Electrochem. Soc. 163 (10) (2016) C649–C658, https://doi.org/10.1149/2.0651610jes.
[48] N.C. Thomas, O.A. Beaumont, G.B. Deacon, C. Gaertner, C.M. Forsyth, A.E. Somers, P.C. Junk, Preparation and structures of rare earth 3-benzoylpropanoates and 3-phenylpropanoates, Aust. J. Chem. 73 (12) (2020), https://doi.org/10.1071/ch20197.
[49] G.O. Ilevbare, G.T. Burstein, The inhibition of pitting corrosion of stainless steels by chromate and molybdate ions, Corros. Sci. 45 (2003) 1545–1569.
[50] N.D. Nam, A. Somers, M. Mathesh, M. Seter, B. Hinton, M. Forsyth, M.Y.J. Tan, The behaviour of praseodymium 4-hydroxycinnamate as an inhibitor for carbon

dioxide corrosion and oxygen corrosion of steel in NaCl solutions, Corros. Sci. 80 (2014) 128–138.

[51] Y. Peng, et al., A study of rare-earth 3-(4-methylbenzoyl)-propanoate compounds as corrosion inhibitors for AS1020 mild steel in NaCl solutions, Corros. Sci. 145 (2018) 199–211, https://doi.org/10.1016/j.corsci.2018.09.022.

[52] N.D. Nam, Q.V. Bui, M. Mathesh, M.Y.J. Tan, M. Forsyth, A study of 4-carboxy-phenylboronic acid as a corrosion inhibitor for steel in carbon dioxide containing environments, Corros. Sci. 76 (2013) 257–266.